Moisture Origin and Meridional Transport in Atmospheric Rivers and Their Association with Multiple Cyclones*

HARALD SODEMANN

NILU, Kjeller, Norway, and Institute for Atmospheric and Climate Science, ETH, Zürich, Switzerland

ANDREAS STOHL

NILU, Kjeller, Norway

(Manuscript received 5 September 2012, in final form 21 December 2012)

ABSTRACT

During December 2006 many cyclones traveled across the North Atlantic, causing temperature and precipitation in Norway to be well above average. Large excursions of high vertically integrated water vapor, often referred to as atmospheric rivers, reached from the subtropics to high latitudes, inducing precipitation over western Scandinavia. The sources and transport of atmospheric water vapor in the North Atlantic storm track during that month are examined by means of a mesoscale model fitted with water vapor tracers. Decomposition of the modeled total water vapor field into numerical water vapor tracers tagged by evaporation latitude shows that when an atmospheric river was present, a higher fraction of water vapor from remote, southerly source regions caused more intense precipitation. The tracer transport analysis revealed that the atmospheric rivers were composed of a sequence of meridional excursions of water vapor, in close correspondence with the upper-level flow configuration. In cyclone cores, fast turnover of water vapor by evaporation and condensation were identified, leading to a rapid assimilation of water from the underlying ocean surface. In the regions of long-range transport, water vapor tracers from the southern midlatitudes and subtropics dominated over local contributions. By advection of water vapor along their trailing cold fronts cyclones were reinforcing the atmospheric rivers. At the same time the warm conveyor belt circulation was feeding off the atmospheric rivers by large-scale ascent and precipitation. Pronounced atmospheric rivers could persist in the domain throughout more than one cyclone's life cycle. These findings emphasize the interrelation between midlatitude cyclones and atmospheric rivers but also their distinction from the warm conveyor belt airstream.

1. Introduction

A large share of precipitation in the midlatitudes is tied to cyclones traveling along the midlatitude storm tracks (Eckhardt et al. 2004). The climatological North Atlantic winter storm track ends over the Scandinavian Peninsula. Its intersection with the steep orographic rise along the Norwegian west coast can lead to extreme precipitation events with severe infrastructure damage (Stohl et al. 2008; Steensen et al. 2011). A statistical analysis by Benestad and Melsom (2002) suggested that anomalously warm SSTs south of Newfoundland could contribute to a positive precipitation trend in western Scandinavia. To understand the physical mechanisms leading to precipitation extremes, however, and to anticipate changes in precipitation in a warming climate, detailed knowledge of the interrelation of evaporative moisture sources for precipitation and atmospheric water vapor (WV) transport processes are needed (Trenberth 1999).

Classically, moisture transport for precipitation in the midlatitudes has been considered from a cyclone-centered perspective. Airflows in extratropical cyclones have been studied since the development of the Bergen school cyclone model (Bjerknes 1919). In the well-known conveyor belt model, which defines airflows in

Denotes Open Access content.

* Supplemental information related to this paper is available at the Journals Online website: http://dx.doi.org/10.1175/MWR-D-12-00256.s1.

Corresponding author address: Harald Sodemann, Institute for Atmospheric and Climate Science, Universitätsstrasse 16, 8092 Zürich, Switzerland.
E-mail: harald.sodemann@env.ethz.ch

DOI: 10.1175/MWR-D-12-00256.1

a quasi-Lagrangian reference frame moving with the cyclone, precipitation is mostly generated by the warm conveyor belt (WCB), a poleward, slantwise ascending airstream rising above the warm front near the cyclone center (Harrold 1973; Carlson 1980; Browning 1990). Rapidly ascending from the surface up to tropopause levels ahead of the cold front within 1–2 days, the WCB generates intense precipitation and condensational latent heating. In this concept, the WCB is responsible for most of the meridional moisture transport with cyclones (Wernli 1997; Eckhardt et al. 2004). As the WCB ascends poleward and generates precipitation, it not only leads to moisture advection, but also to the drying of air masses.

At the end of the North Pacific storm track, a configuration similar to that in the North Atlantic exists where the atmospheric flow intersects the steep orographic rise in western North America. In that region, heavy precipitation events and flooding have often been investigated within the framework of so-called atmospheric (originally tropospheric) rivers (ARs), narrow filaments of high vertically integrated WV flux extending from the (sub)tropics to the midlatitudes (Newell et al. 1992; Zhu and Newell 1998). The concept states that five or six major ARs are present in each hemisphere most of the time, with moisture fluxes comparable to some of the major terrestrial rivers. Vertically integrated WV (IWV), which is readily available from passive microwave satellite imagery, can be used as a proxy for vertically integrated WV fluxes, as validated in three field campaigns involving research aircraft (Ralph et al. 2004, 2006, 2011). An impressive visual characteristic of ARs is that they can be clearly identified as long, narrow bands of high IWV extending from the (sub) tropics to the midlatitudes on IWV maps.

In this alternative concept, attention is shifted away from the role of individual cyclones and their role for meridional moisture transport. Thereby the important connection between upper-level dynamics and lower-tropospheric transport may be overlooked. Furthermore, the term atmospheric river suggests that atmospheric moisture transport occurs in a two-dimensional riverlike flow from the (sub)tropics to the mid- and high latitudes, with ensuing precipitation extremes when the flow intersects the topography. The three-dimensional ascent of airstreams, which is a prominent aspect of the conveyor belt model, disappears if only a vertically integrated AR perspective is considered.

The AR perspective can however be very useful when these caveats and limitations are properly taken into account. In particular, the AR concept has proven to be very valuable in order to focus on the role of atmospheric moisture transport for heavy precipitation events (Ralph et al. 2006). In a study by Stohl et al. (2008) an AR contributed to extreme precipitation at the Norwegian west coast. In that particular case the extratropical transition of two former hurricanes also played an important role in bringing an extensive warm and moist air mass from the subtropics to the midlatitudes, thereby fueling the precipitation event. Thanks to its simplicity compared to the more involved conveyor belt model, the AR concept greatly facilitates interfacing with other disciplines, such as hydrology. Neiman et al. (2010), for example, found from analyzing a 30-yr period that most annual peak runoff events at four major watersheds along the U.S. West Coast were related to ARs. In Great Britain, ARs have been related to the 10 largest winter floods since 1970 (Lavers et al. 2011). Here, we attempt to obtain a synergistic view on meridional moisture transport in the midlatitudes that takes the role of cyclones and the dynamics at upper levels into account, while at the same time taking advantage of the intuitiveness of the AR concept.

Bao et al. (2006) were the first to investigate moisture origin in ARs. Their findings pointed to a dominant role of moisture convergence for forming AR-like bands of high IWV. Near a cyclone, moisture convergence took place in the WCB circulation, while farther away moisture convergence occurred along the trailing cold front. The direct advection of moist air from the tropics to midlatitudes appeared to be the exception. A quantitative description of the relative importance of the processes relevant for AR formation was however unavailable from their method. Stohl et al. (2008) investigated the source regions of precipitation in Norway climatologically with a Lagrangian moisture source diagnostic and found regular contributions from latitudes between 20° and 40°N. In a further climatological study for the Northern Hemisphere based on backward trajectories, Knippertz and Wernli (2010) examined the poleward moisture transport by so-called tropical moisture export events, defined as a large WV flux reaching from south of 20°N to north of 35°N. These events are rooted in the tropics, and at the southern end may be related to the tropical moisture conveyor belts in which most of the moisture transport takes place above the boundary layer (Bao et al. 2006; Knippertz and Martin 2007). All of these studies support the view that moisture is transported from the (sub)tropics to the midlatitudes in distinct, individual plumelike events.

In simulations of idealized cyclogenesis in a mesoscale numerical weather prediction (NWP) model, Boutle et al. (2011) found that large-scale ascent in the WCB and shallow convective processes contributed about equally to free tropospheric moisture, which then could be subject to long-range advection. Their numerical planetary boundary layer tracer did, however, not allow for tracking the WV during subsequent phase transformations, in particular precipitation formation. Thus, the actual evaporative sources of the moisture in ARs

and the role of moisture removal due to precipitation have so far not been revealed in detail.

A powerful numerical tool within the framework of an Eulerian model to investigate source–receptor relationships of moisture are artificial WV tracers (WVTs). Released by evaporation from the surface or during advection of WV through specified boxes, WVTs are transported in a fully independent secondary water cycle and do not interfere with the simulated meteorology itself. By means of this so-called water vapor tagging, it can be investigated where water vapor that evaporated in a predefined source region returns to the surface as precipitation. Initially, WVTs were introduced for general circulation models (Joussaume et al. 1984; Koster et al. 1986; Numaguti 1999; Bosilovich and Schubert 2002). Sodemann et al. (2009) recently implemented water vapor tagging into a limited-area NWP model. This allows for the analysis of simulated moisture transport and moisture source contributions to precipitation at high resolution, including all relevant parameterized processes, such as cloud microphysics. Recently, the same WVT approach has also been used to investigate the coupling between surface evaporation and moisture advection for a case of extreme precipitation in the Mediterranean (Winschall et al. 2012). In this study we apply the water vapor tagging to investigate the moisture sources and composition for several AR events.

During the period investigated here (December 2006), a relatively large number of cyclones traveled along the North Atlantic storm track and brought warm and moist air masses with above-normal precipitation totals to many parts of the Scandinavian Peninsula. The preceding fall season of 2006 was the warmest on record in Europe, which may partly have been influenced by strong positive SST anomalies in the eastern North Atlantic (Cattiaux et al. 2009). The synoptic situation in the North Atlantic during much of December 2006 was characterized by many small cyclones, large anticyclones, narrow upper-level troughs, and often a meridionally oriented upper-level jet. In their idealized life cycle framework, Thorncroft et al. (1993) termed such a synoptic evolution life cycle 1 (LC1) or an anticyclonic life cycle. In contrast, during the life cycle 2 (LC2), or the cyclonic life cycle, the tropopause jet is more meridionally confined, cyclones are larger, and the upper-level troughs broader, as was the case at the beginning and end of December 2006. While that month cannot be considered as climatologically typical, the high frequency of storms allowed investigation of several similar cases over a short time period, as well as their joint impact.

In this study we investigate the moisture origin and moisture transport within and induced by cyclones in the North Atlantic storm track, and the resulting contribution to precipitation in western Scandinavia during December 2006 by means of WVTs in a limited-area NWP model simulation. In sections 3a and 3b we provide a synoptic overview and analyze how the meridional moisture transport is linked to the upper-tropospheric circulation in the study domain. Using ocean evaporation tracers from different latitude bands, the moisture origin for precipitation events connected to atmospheric rivers is investigated in sections 3c and 3d. Section 3e presents the horizontal and vertical structure of the oceanic tracer composition in the regions of strongest meridional water vapor transport. The temporal evolution of the moisture source composition near cyclone centers and farther downstream are investigated in section 3f. Section 4 discusses the circumstances under which several cyclones sequentially interact to enhance the poleward transport of WV. Conclusions are drawn in section 5.

2. Data and methods

a. Meteorological data

Daily mean sea level pressure (SLP), 2-m temperature, and 24-h accumulated precipitation data were acquired for three stations—Flesland near Bergen (60.29°N, 5.23°E, 48 m MSL), Tromsø (69.65°N, 18.94°E, 100 m MSL), and Oslo-Blindern (59.94°N, 10.72°E, 94 m MSL)—using the eKlima portal of the Norwegian Met Service (http://eklima.met.no). These stations were selected to cover the main meteorological features in southwestern, northern, and southeastern Norway, respectively. Six-hourly meteorological analysis data were retrieved for the period 15 November 2006–5 January 2007 from the European Centre for Medium-Range Weather Forecasts (ECMWF) at a spectral resolution of T799 and 91 vertical levels, and interpolated onto a $1.0° \times 1.0°$ horizontal grid spacing.

b. CHRM model and water vapor tagging method

The High-Resolution Model (HRM) is a hydrostatic limited-area NWP model that had originally been part of the German Weather Service's operational weather forecasting model chain as the Europa Modell (Majewski 1991). Later on, a climate component was added, enabling the model to run seasonal and multiyear integrations (Schär et al. 1999). This so-called climate HRM (CHRM) has been used extensively for climate simulations and process studies in the midlatitudes and was, until recently, in operational use by several national meteorological services. CHRM uses a rotated coordinate system with an Arakawa C grid in the horizontal and hybrid sigma–pressure coordinates in the vertical direction. The bulk microphysics scheme follows Kessler (1969) and Lin et al. (1983), and for convection the Tiedtke (1989) mass-flux

scheme is used. A Dickinson (1984) soil model with three layers is used at the surface.

Numerical water vapor tracers have been used by a number of authors in global models to diagnose the sources and transport pathways of water vapor (Joussaume et al. 1984; Koster et al. 1986; Numaguti 1999; Bosilovich and Schubert 2002). CHRM tagging is the first limited-area NWP model capable of advecting water vapor tracers through its own complete secondary water cycle (Sodemann et al. 2009).[1] The tracer water is released either through evaporation from predefined surface areas, or introduced into the domain by advection at the boundaries. The multidimensional positive-definite advection transport algorithm (MPDATA; Smolarkiewicz 2006) is used for advecting both the WV tracers and the total WV field. In this study a consistent advection scheme is used for the tracers and total WV field. This new modification leads to substantially better conservation of cloud water in comparison to the previous CHRM-tagging version, which applied a leapfrog scheme for total WV advection and MPDATA for the tracer advection. In all parameterized subgrid-scale processes that involve phase changes, the transfer rates of tagged moisture from one phase to another are considered proportional to the fraction of tagged water times the respective total transfer rate. Precipitation receives the tag from the vapor it condenses from. Further details on the tagging implementation are available in Sodemann (2006) and Sodemann et al. (2009). In this study a coding error has been corrected in the parameterization of the evapotranspiration of tagged WV from land surfaces, which leads to an increase in tagged land evapotranspiration compared to the previous version (Winschall et al. 2012). A further important new modification of the model is the deactivation of the calculation of modified turbulent transfer coefficients in the presence of clouds, which had led to a violation of mass conservation within clouds. With these modifications, the fraction of WV not assigned to any tracer (see section 2c), which is due to numerical diffusion and numerical inconsistencies, remains below 1%–2% for WV and cloud water throughout the simulation period for the whole domain, and below 5%–10% for local precipitation. For ease of interpretation, all tracer results in this paper have been scaled relative to the total known amounts of WV and precipitation.

c. Simulation setup and tracer experiments

We employ the CHRM WV tracers to follow the moisture evaporating from oceanic source regions to target domains in southern and northern Norway. The simulation domain includes most of the North Atlantic winter storm track region (Fig. 1). ECMWF analysis data have been supplied at the boundaries and for the nudging (see below) continuously by interpolating between the 6-hourly analyses. The CHRM grid spacing is 0.5° × 0.5° in the horizontal, with 40 vertical levels. During the 1.5-month integration starting at 0000 UTC 15 November 2006, a variable nudging of the wind fields has been applied, as described in section 2d.

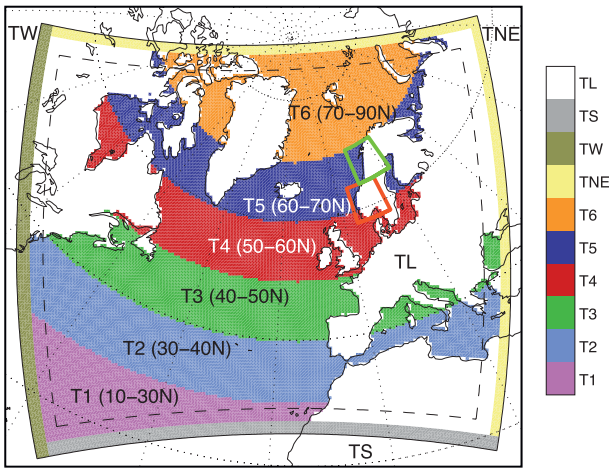

FIG. 1. Calculation domain of the CHRM model (solid black line) and interior model domain (dashed black line). Colors show moisture source tracers released by surface evaporation from every 10° latitude band of ocean area (T1–T6), land (TL, here plotted in white), and from advection through the southern (TS), western (TW), and northeastern (TNE) boundaries reaching from the bottom to top of the model domain. Initial atmospheric tracer (TA) is not displayed. Boxed areas over Scandinavia denote the target domains of northern Norway (green) and southern Norway (red).

Six oceanic source regions for WV tracer evaporation have been defined in the North Atlantic domain, by means of four 10°-wide latitude bands from 30° to 70°N, plus the regions south of 30°N and north of 70°N (Fig. 1, shaded areas). Tracers are numbered from south to north as T1–T6. Evapotranspiration from all land regions is tagged by one additional tracer (TL). Furthermore, at the boundaries, atmospheric inflow is tagged from the south (TS), west (TW), and north and east (TNE). All moisture present in the atmosphere at initialization time has unknown sources and is tracked as an additional tracer labeled TA. The sum of all tracers thus allows us to calculate the fraction of unassigned WV. Two target domains have been defined for analyzing moisture sources for precipitation over western Scandinavia. The northern Norway (NN) domain covers the region 63°–72°N and 8°–26°E (Fig. 1, green box), while southern Norway (SN) is defined here as the region 58°–63°N and 4°–14°E (Fig. 1, red box). This choice

[1] A further tagging implementation has now also been completed for the widely used Consortium for Small-Scale Modeling (COSMO) model (Winschall 2012).

has been based on the very different weather conditions often prevailing in these regions during the study period (see section 3a).

d. Tagging spinup

During the spinup of the tagging simulation, the moisture of tracer TA residing in the domain initially with unknown evaporative source regions is continuously replaced by tracer moisture with known origin through evaporation from the surface and advection at the boundaries. We performed a two-stage simulation, consisting of a spinup and an analysis period. The period 15–30 November served as a spinup period to remove as much as possible of the moisture with unknown sources that is present in the domain initially (tracer TA), while the period 1–31 December has been used for further analysis. At the end of the spinup period less than 0.5% of the original TA tracer was left inside the model domain. During the spinup period model winds were nudged to the 6-hourly ECMWF winds interpolated in time with a fairly strong relaxation rate of $\gamma = 10^{-4}$ s^{-1}. This tied the simulation closely to the ECMWF analyses while allowing spinup of the tracer distribution in the model domain. We did not nudge temperature and humidity fields to avoid a too direct interference with the model's hydrological cycle. For the analysis period, the relaxation rate of the wind fields was then lowered to $\gamma = 10^{-5}$ s^{-1} to allow the model to develop its own internal representation of the water cycle. At the same time, the nudging ensured that the model would not too strongly deviate from the analysis, allowing for a meaningful comparison to station data.

3. Results

a. Meteorological evolution in Norway during December 2006

An almost continuous sequence of cyclones brought warm and moist air to all of western Scandinavia during December 2006. Precipitation was 100%–200% above average in many regions of Norway, temperatures were the warmest for a December since the beginning of recorded temperatures, and new temperature and precipitation records were set at many weather stations (Meteorologisk Institutt 2007). Similar weather continued into January and February 2007 (Luterbacher et al. 2007), with an extreme precipitation event taking place in central Norway at the end of January (Steensen et al. 2011). This anomalous weather pattern is reflected in a high value of the SLP-based winter season (December–March, DJFM) mean North Atlantic Oscillation (NAO) index of +1.83 (Osborn et al. 1999; updated as described online at http://www.cru.uea.ac.uk/~timo/datapages/naoi.htm). In the following, the regional model simulation is briefly validated by a comparison to the observations at three meteorological stations in Norway.

Flesland (Bergen Airport, 48 m MSL) is a weather station situated along the west coast of Norway, but at some distance from the steepest orographic rise. Given our fairly coarse model resolution, comparison with the simulation results is more meaningful for Flesland than for the better known nearby station Bergen-Florida, which has one of the highest climatological precipitation totals in Norway (2250 mm annual mean and 235 mm December mean, at Flesland these numbers are 1815 mm and 189 mm, respectively), partly due to precipitation enhancement along the steep orographic rise to 600-m altitude within a very short distance from the weather station. Due to the frequent landfall of cyclones at the end of the North Atlantic storm track, the climatological mean 2-m temperature T_{2m} during December of 1.8°C is relatively high for the station's latitude. During December 2006, however, T_{2m} was 4–7 K above normal on most days (Fig. 2a, thick line). A warm period until 17 December was accompanied by intense precipitation events, with 52.4-mm precipitation in 24 h on 11 December (Fig. 2g, open bars). SLP was fairly low during the first 2 weeks of December, with a minimum below 971 hPa on 4 December (Fig. 2d, thick line). While SLP increased during the second half of December 2006, precipitation amounts still remained substantial. The precipitation total at Flesland during December 2006 amounted to 323.5 mm, which is 70% more than the climatological mean. The thin lines in Fig. 2 show the results of the nudged regional NWP model simulation, taken from averaging all land grid points within 60 km from the station location. The simulated T_{2m} at Flesland shows a very large warm bias during a cold episode after 18 December, while the overall evolution is captured well (Fig. 2a). For SLP, correspondence between the model and observations is very good (Fig. 2d). While the model is not able to capture the precipitation amounts at Flesland at the 0.5° × 0.5° horizontal grid spacing employed here, precipitation timing has been simulated reasonably well (Fig. 2g). The exception is the period 20–25 December, when a significant precipitation event is simulated to be much weaker than observed. Detailed inspection of the simulation shows that the precipitation area, connected to a landfalling AR (see section 3b), was displaced slightly northeastward compared to the actual weather evolution.

The station Oslo-Blindern (94 m MSL) is situated about 300 km east of Bergen, with less exposure to landfalling storms from the west. During the first half of December, T_{2m} was 6–8 K warmer than normal, which was accompanied by 22.6 mm day^{-1} of precipitation on 8 December, and a drop in SLP to 981 hPa (Figs. 2b,e,h).

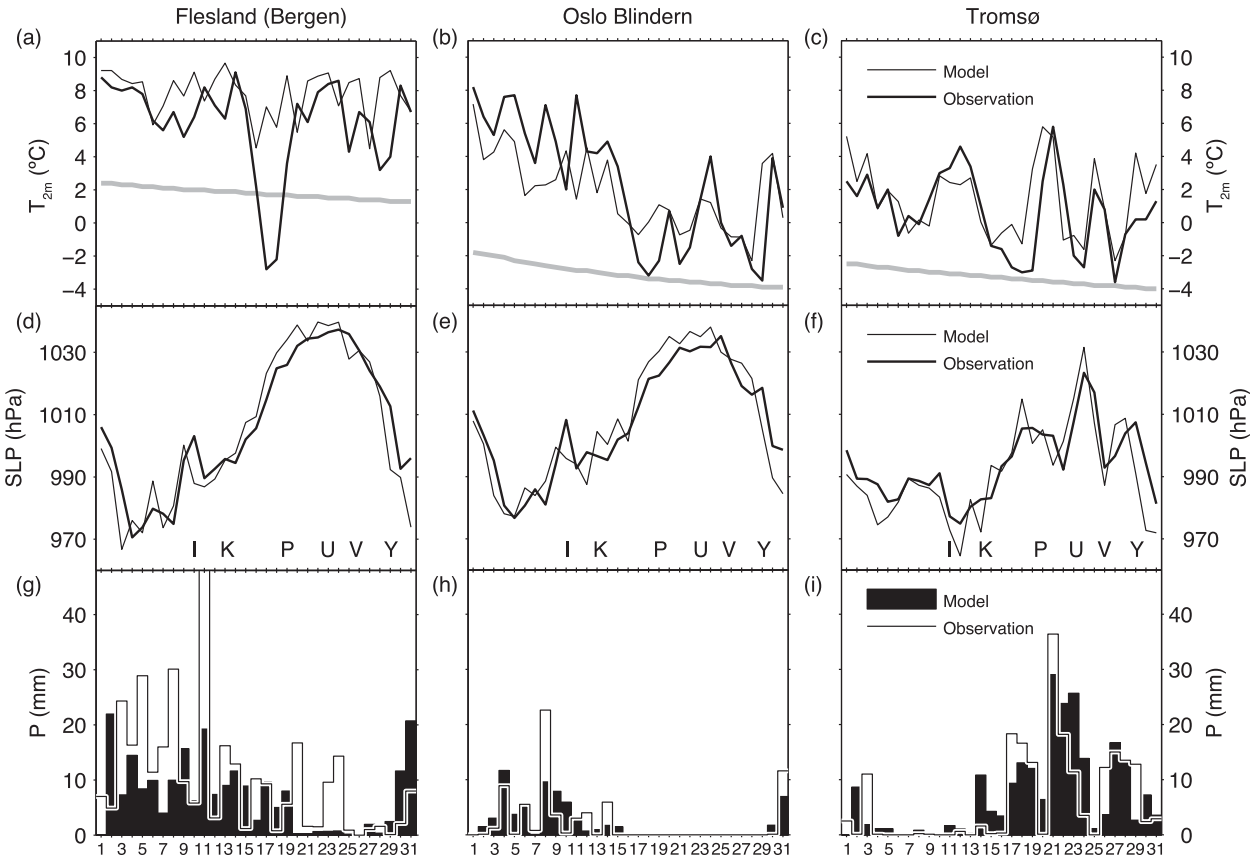

FIG. 2. Time series of simulated and observed meteorological variables at the stations (left) Flesland near Bergen, (middle) Oslo-Blindern, and (right) Tromsø during December 2006. (a)–(c) Observed (boldface line) and simulated (thin line) daily mean 2-m temperature (°C) compared to the climatology (thick gray line). (d)–(f) Observed (boldface line) and simulated (thin line) daily mean SLP (hPa). (g)–(i) Simulated (filled area) and observed (lines) 24-h accumulated precipitation (mm). Letters in (d)–(f) refer to labeled cyclones in Fig. 3.

The second half of December was fairly dry at that station, as a high pressure system influenced southeastern Norway, and temperatures were closer to the climatological mean. For T_{2m} the trend is captured well by the simulation, while the variability is too low (Fig. 2b). For precipitation, agreement between the model and observations is very reasonable, both in terms of timing and magnitude.

At Tromsø, several prolonged episodes with temperatures up to 9 K above the climatological mean occurred during December 2006, again accompanied by intense precipitation of up to 36.3 mm on 21 December (Figs. 2c,i). Precipitation episodes coincided with marked drops in SLP on 21 and 27 December, indicating the proximity of low pressure systems (Fig. 2f). Interestingly, most precipitation was recorded in Tromsø when Bergen-Florida and Oslo-Blindern received little precipitation. The simulated T_{2m} matches observations fairly well, again with a slight warm bias during cold episodes. For precipitation, the model underestimates high daily precipitation totals, while the timing and duration of the simulated precipitation events match very well with the observations.

b. *Evolution of the synoptic situation in the study domain*

The covariance between SLP and precipitation in Fig. 2 suggests that precipitation is largely driven by cyclone activity during the study period. Indeed, about six cyclones made landfall in Norway during the study period, out of a total of 29 cyclones identified in the simulation domain during December 2006. In the following, the evolution of the meteorological situation is described with an emphasis on moisture advection to the target domains.

Figure 3 displays the upper-level flow configuration at four selected times in terms of the isentropic potential vorticity (PV, shaded) and wind velocity at the 325-K potential temperature surface as contours in the panels on the left. On the right in Fig. 3, the meteorological

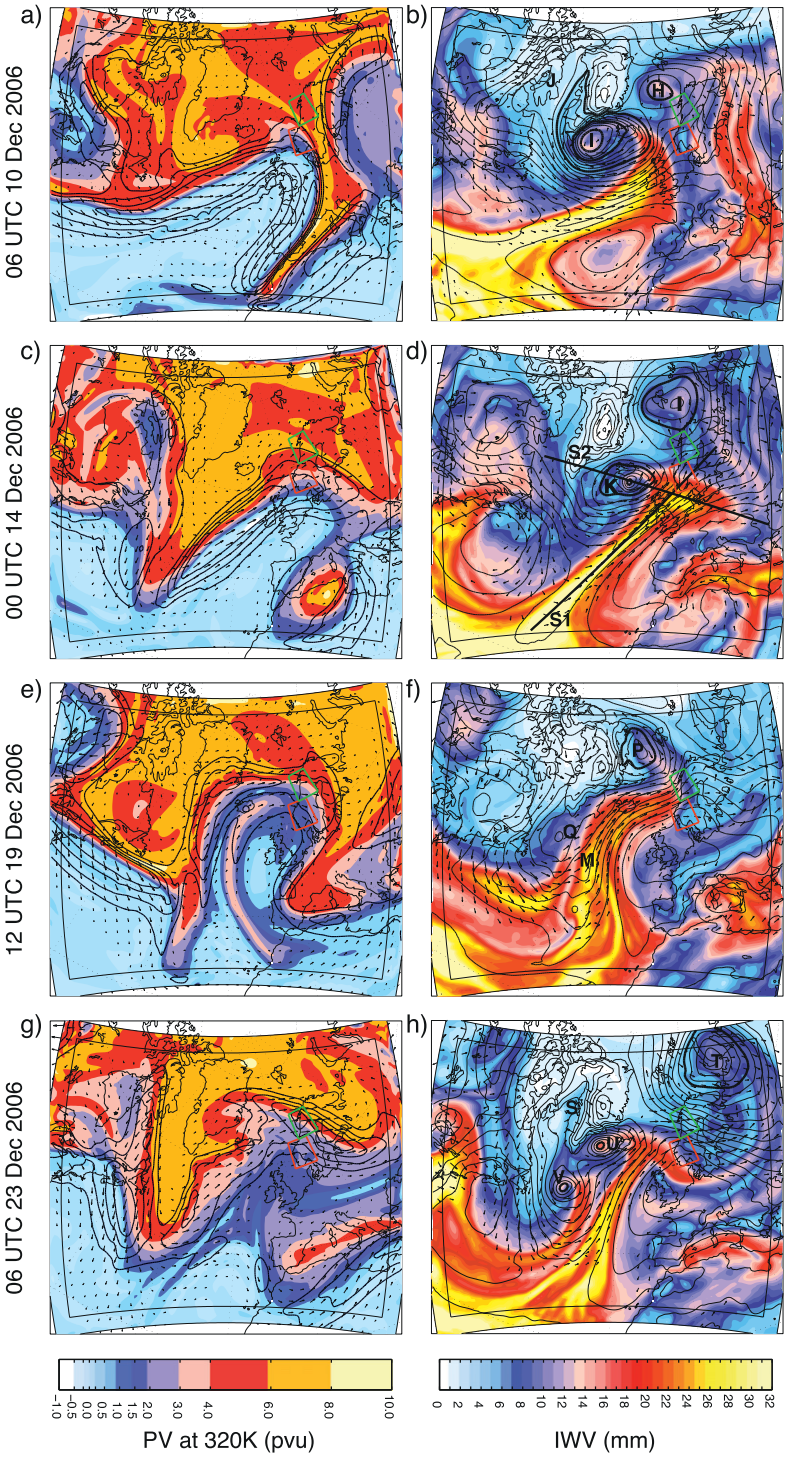

FIG. 3. Meteorological configuration (left) at the tropopause and (right) in the lower troposphere at 0600 UTC 10 Dec, 0000 UTC 14 Dec, 1200 UTC 19 Dec, and 0600 UTC 23 Dec 2006 as simulated by the CHRM model. (a),(c),(e),(g) Isentropic potential vorticity [PV, in potential vorticity units (PVU, shading, 1 PVU = 10^{-6} K m^2 kg^{-1} s^{-1})], wind direction (arrows), and wind speed (m s^{-1}, black contours at 30, 40, 50, and 60 m s^{-1}) on the 325-K isentrope. (b),(d),(f),(h) IWV (mm, shading), SLP (hPa, black contours, intervals of 5 hPa between 1040 and 950 hPa, with thick contours at 980, 960, and 940 hPa), and wind vectors at 850 hPa (arrows). Black letters refer to tracked cyclones (see text). Cross sections S1 and S2 indicated in (d) are shown in Fig. 7.

situation in the lower troposphere is depicted as vertically integrated WV between 200 hPa and the surface (shaded, mm), SLP (contours, hPa), and winds at 850 hPa (arrows). Cyclones are labeled alphabetically by black letters following their sequence of occurrence in the simulation domain. When viewed jointly with the low-level winds, the direction and magnitude of the water vapor fluxes can be estimated from the IWV field. We use IWV as a proxy for water vapor fluxes throughout this manuscript.

During 1–7 December 2006, a mostly zonally oriented jet at upper levels, combined with a pronounced stationary low pressure system centered north of the British Isles, dominated the atmospheric circulation pattern in the model domain (not shown; see the online supplemental material). At 0600 UTC 10 December 2006 the jet stream had attained a slight meridional orientation along a pronounced upper-level ridge (Fig. 3a), leading to the advection of a large air mass of high IWV toward the British Isles (Fig. 3b). South of Greenland, cyclone I intensified rapidly, reaching a minimum core pressure below 960 hPa. The area of high IWV apparently extended from poleward subtropical latitudes and fed into the cyclone's frontal system. Despite indications of evaporation in the cold sector, a fairly sharp gradient existed between the pre- and post-cold-frontal air (Fig. 3b). During the following 24 h, the frontal system of cyclone I passed over southern Norway, bringing 52.4 mm day^{-1} of precipitation to Flesland (Fig. 2g). With its broad, mostly zonally oriented tropopause-level structure and the dominance of a single large cyclone in the area, this period resembles the LC2 wave breaking category.

At 0000 UTC 14 December, the upper-level jet had become more meridionally oriented in a subsequent Rossby wave breaking event (Fig. 3c). A fairly narrow, elongated band of high IWV was present at that time (Fig. 3d), reminiscent of an AR. The frontal area of cyclone K was broad near the occlusion and was wrapped partly around the cyclone center. As the cyclone moved into northern Norway during the following day, mean SLP remained low at 983 hPa in Tromsø (NN in Fig. 2f), while precipitation mostly fell in southern Norway.

At 1200 UTC 19 December, a pronounced Rossby wave with a partly meridional jet was present at upper levels (Fig. 3e), which had favored northward advection of moist subtropical air masses in a large area of the eastern North Atlantic (Fig. 3f). Cyclone P with a core pressure of 973 hPa had moved poleward along the east coast of Greenland, followed by a long trailing band of high IWV values (Fig. 3f). During the next 12 h, cyclone P traveled north to Svalbard, and became detached from the band of high IWV. The moist air mass caused precipitation first in southern Norway, then in northern Norway during the next 48 h. At Flesland, observed precipitation was 16.7 mm day^{-1} on 20 December, which was missed in the simulation due to a northward displacement of the AR (Fig. 2g). At Tromsø the precipitation event was more pronounced, with more than 13 mm day^{-1} precipitation on three consecutive days and a maximum of 36.4 mm day^{-1} on 21 December (Fig. 2i). In the following 12 h, the remnants of cyclone M, which had developed in the subtropics, were incorporated into the IWV plume. At the same time cyclone Q had formed from a frontal wave instability in the IWV plume near 55°N (cf. Ralph et al. 2011), generating another filament of high IWV off Newfoundland from evaporation behind the cold front, which is incorporated into the large subtropical moisture excursion downstream. In the Thorncroft et al. (1993) cyclone life cycle classification, due to the meridionally oriented jet and the presence of many small cyclones, this flow configuration is similar to the LC1 type.

By 0600 UTC 23 December cyclone U had intensified and moved into the Greenland Sea west of Iceland, attaining a minimum core pressure of 977 hPa (Fig. 3h). A double frontal structure had developed from the remnants of the previous IWV filament adopted by cyclone U and the developing frontal system of cyclone V, which later on become indistinguishable from one another. As cyclone U moved north of Iceland during the next 12 h, steered by the northeast-oriented upper-level jet (Fig. 3g), its frontal system made landfall in southern Norway with direct onshore flow from the southwest, shedding 14.3 mm day^{-1} precipitation at Flesland (Fig. 2h). Onshore flow remained stationary at about 64°N until 0000 UTC 25 December, as cyclone V split southeast of Greenland and moved north along the east coast, dragging a narrow IWV filament behind it. While further intensifying, cyclone V moved north of Svalbard before it slowly filled and drifted southeast, its trailing frontal system precipitating out over northern Norway after 26 December with above 12 m day^{-1} of precipitation at Tromsø on four consecutive days (Fig. 2c).

At 1800 UTC 29 December, the upper-level jet attained a zonal orientation again, and an intense cyclone Y had developed in warm and moist air with a large area of high IWV ahead and south (see the online supplemental material). While further intensifying during the next 12 h, cyclone Y moved its center to Iceland and became the single dominant low pressure pattern over the North Atlantic. The band of high IWV was pushed southeast and crossed Norway during the following 24 h, with observed precipitation of over 8.0 mm day^{-1} at Flesland and 11.6 mm day^{-1} at Oslo-Blindern (Figs. 2g,h). Similar to the period before 10 December, this flow configuration can be classified as an LC2 case.

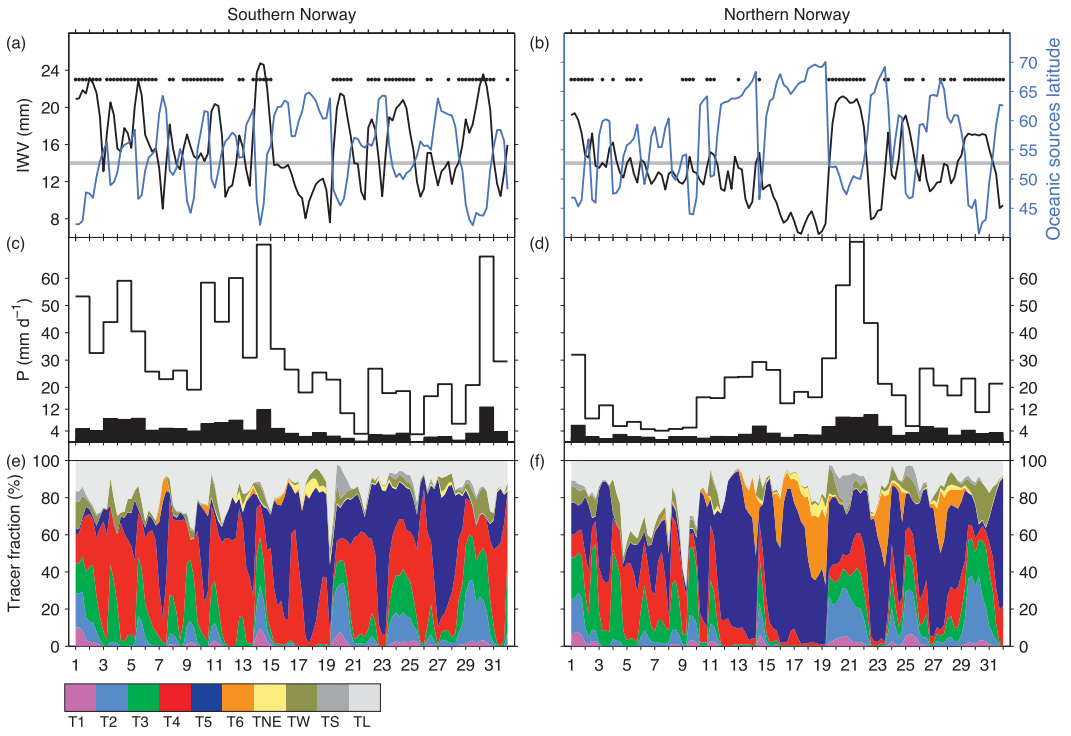

FIG. 4. Time series of AR conditions and simulated precipitation origin in the (left) SN and (right) NN domains. (a),(b) Maximum IWV (black line, mm) and oceanic sources latitude (blue line, ° latitude) in the respective domains at a 6-hourly interval. Thick gray line denotes the 14-mm threshold for AR conditions, and black dots denote AR periods. (c),(d) Simulated daily maximum (open bars) and mean (filled bars) accumulated precipitation in the respective domain (mm day^{-1}). (e),(f) Tracer fractions for the domain average precipitation at a 6-hourly interval (%).

c. *Temporal sequence of oceanic moisture tracer contributions in the target domains*

From the previous discussion, it could be seen that precipitation in western Scandinavia coincided with poleward extensions of high IWV bands [for reasons of simplicity referred to as atmospheric rivers (AR) here] that appeared to contribute to the WCB airstream of cyclones. However, these ARs could not always be related to exactly one cyclone and apparently existed longer than individual cyclones. Instead, the precipitation generating WCBs of individual cyclones seemed to feed on the ARs but consumed only part of the available moisture. At the same time, narrow IWV filaments formed by evaporation in the cold sector were fused into the ARs at the upstream edge (e.g., Figs. 3f,h). A single AR thus could be supply the moisture for several small cyclones, which were spawned along and north of the AR. By means of the WV tracers, we now focus on the question of how the origin of the precipitation in western Scandinavia varied in the presence of ARs.

To identify periods when ARs contributed a significant share to total precipitation in one of the target regions, we defined AR periods when at least one grid box was above a threshold value of 14-mm IWV over land within the target regions. The 14-mm threshold value was chosen after careful testing and inspection of all individual cases of landfalling ARs in Norway during this period. Ralph et al. (2004) used a threshold value of 20 mm for the definition of atmospheric rivers at the eastern North Pacific at latitudes of ~30°–40°N, but due to the higher latitudes considered here, and since only grid points over land (and hence with underlying topography) are evaluated, it is reasonable to choose a lower threshold value for AR conditions. Figure 4 shows how the AR identification depends on the threshold value. Whenever the maximum IWV in a target region exceeds 14 mm (Figs. 4a,b, gray line), an AR period is identified (Figs. 4a,b, black dots). Fairly strong variability of IWV on a 3–5-day time scale is apparent in the two domains. Several of the ARs roughly precede or coincide with peaks in mean and maximum precipitation in the domains, for example, on 14–15 December in southern Norway and on 21–22 December in northern Norway (Figs. 4c,d). Figures 4e and 4f show the relative contribution of all moisture source tracers to the 6-hourly precipitation total in each domain. While the highest contributions come from the regions T4 (red) in SN and T5 (dark blue) in NN,

TABLE 1. Correlation of each water vapor tracer (Tx) contribution time series with mean IWV in the NN and SN domains during December 2006 at a 6-h time interval. Significant correlations at $p < 0.001$ are shown in boldface.

	T1	T2	T3	T4	T5	T6	TNE	TW	TS	TL
NN	**0.6346**	**0.7101**	**0.5128**	0.2374	**−0.4250**	**−0.4762**	**−0.4249**	**0.4267**	**0.6094**	−0.1901
SN	**0.6079**	**0.6586**	**0.7098**	−0.1921	**−0.5557**	−0.2528	**−0.4050**	**0.5517**	**0.3995**	−0.0971

during AR periods and peaks in maximum precipitation in both domains substantial contributions come from ocean sectors T1–T3 (pink, light blue, green, respectively). In these events the three southerly tracers can contribute up to 60% of the total precipitation. On the other hand, during some non-AR periods in NN (e.g., 15–19 December), local and northerly tracers (T5, T6) contribute most of the precipitation water.

A correlation analysis between the maximum IWV in the NN and SN domains and the respective time series of each tracer's relative precipitation contribution reveals tracer T2 (30°–40°N) as most influential in NN, while T3 (40°–50°N) has the strongest correlation in SN (Table 1). Weaker yet significant positive correlations are found for T1–T3 as well as the boundary tracers TW and TS in both domains. Local tracers are negatively correlated with IWV (T5 for SN, T5 and T6 for NN), emphasizing the role of long-distance advection for high IWV values over Norway. The oceanic source mean latitude, constructed from the precipitation-weighted center latitude of the oceanic source regions of T1–T6, is clearly anticorrelated with the maximum IWV in both domains, consistent with the correlation analysis (Figs. 4a,b, blue line). During AR conditions, the mean oceanic source region can very rapidly shift to locations 15°–20° farther south than during non-AR conditions.

d. Total oceanic moisture tracer contributions to target domain precipitation

The most important moisture contributor to precipitation in SN during the whole study period is T4 (50°–60°N) with 36.3% (Table 2, red area in Fig. 4e). The more southerly ocean regions T1–T3 in combination contribute 21.7%. Further large contributors are land regions (TL) and tracer T5 (60°–70°N) with 19.6% and 15.2%, respectively. For NN, region T5 is the dominant contributor with 36.1%. Here, T1–T3 contribute 24.1% to the precipitation total. Further substantial contributions are from TL (13.6%) and T4 (13.1%). Essentially, this means that the majority of the precipitation in the target domains is contributed by moisture evaporating at local or nearby latitudes. However, since precipitation formation is a highly nonlinear process, the relevance of the remaining moisture from farther south may be larger than their relative contribution to total precipitation suggests. For example, enhanced moisture content above the freezing level will be important for the formation of ice particles, which would allow for more efficient precipitation formation in the atmospheric column below than when only warm-cloud microphysics are involved.

The total source region contributions are further investigated by separating the precipitation origin for AR and non-AR conditions. During AR conditions, as has already been suggested by the oceanic source mean latitude time series (Figs. 4a,b), persistently higher contributions from ocean sources south of 60°N in SN and NN are identified (Figs. 5a,b). During AR conditions in SN, the southerly tracers T1–T3 increase their contributions by factors of 10–20 (Table 2). Tracer T5 shows the most pronounced decreases during AR conditions. The more distant boundary tracers TW and TS increase during AR conditions. For NN, tracer T5 also decreases most markedly during AR conditions, while the southerly tracers T1–T3 increase by a factor of 2–5. Moisture from outside the western and southern model boundaries (TW, TS) contributes more to AR precipitation events (Fig. 5b). The less clear-cut separation between AR and non-AR contributions for the NN domain could indicate that the 14-mm threshold value may be too high for these latitudes. Overall, this analysis quantitatively consolidates the previous picture that more long-range transport of moisture from southerly latitudes occurs during AR conditions.

When considering histograms of the 6-hourly gridpoint precipitation rate for the AR and non-AR categories (Figs. 5c,d), it is apparent that the precipitation characteristics are markedly different for the AR versus non-AR conditions. First, there are fewer grid points with no precipitation [<0.1 mm $(6\ \text{h})^{-1}$] during AR

TABLE 2. Contribution of all water vapor tracers (Tx) to the total accounted precipitation in the NN and SN domains during December 2006 (%), also separated into atmospheric river conditions (AR) and non-AR conditions (nAR). Contributions from tracer TA are below 0.1% for all cases.

	T1	T2	T3	T4	T5	T6	TNE	TW	TS	TL
NN all	1.8	10.0	12.3	13.1	36.1	4.8	1.1	4.8	2.5	13.6
NN AR	2.8	16.1	15.7	14.2	26.4	2.4	0.7	6.1	4.4	11.0
NN nAR	0.6	3.5	8.6	11.9	46.5	7.3	1.4	3.3	0.4	16.5
SN all	1.4	5.5	14.8	36.3	15.2	0.4	0.9	5.2	0.6	19.6
SN AR	2.0	9.5	20.2	32.7	8.2	0.1	0.6	6.8	1.3	18.6
SN nAR	0.1	0.5	2.0	37.3	38.9	1.1	1.8	1.7	0.1	16.7

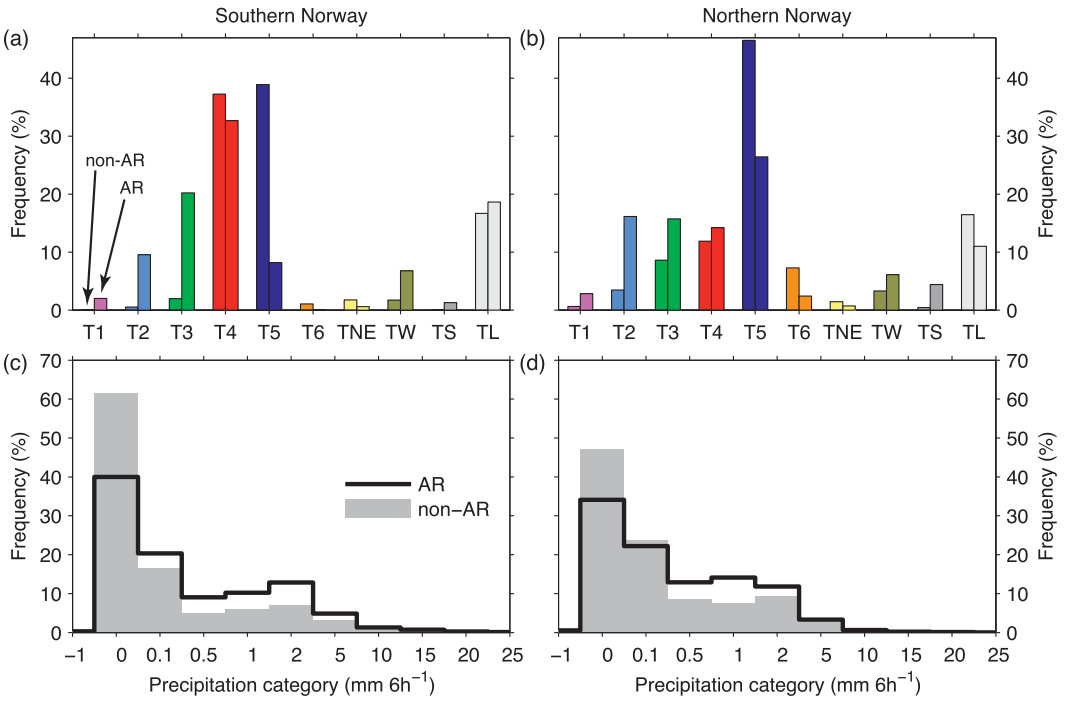

FIG. 5. Fraction of total precipitation contributed by the moisture source tracers (%) during AR and non-AR conditions for (a) SN and (b) NN. Histograms of categorized 6-hourly precipitation at all land grid cells for AR periods (black line) and non-AR periods (gray area) in (c) SN and (d) NN.

conditions in both domains. Second, the strongest increase is for grid points with medium precipitation rates [0.5–2 mm (6 h)$^{-1}$], and less for higher precipitation rates. Precipitation is thus more widespread and more intense during AR conditions, but not necessarily extreme. Overall, in SN precipitation is 2.9 mm (6 h)$^{-1}$ higher during AR compared to non-AR conditions, yet with a large variability (Table 3). For NN, the precipitation increase during AR conditions is relatively small [from 3.4 to 3.7 mm (6 h)$^{-1}$]. The T_{2m} values are markedly different, with 1.8 K warmer conditions for AR conditions in SN and 1.4 K in NN (Table 3). AR and non-AR conditions thus mark periods when the study domains are under the influence of distinct air masses that have very different moisture source, temperature, and precipitation characteristics. It is now further investigated how the AR air masses obtain these distinct characteristics.

e. *Structures of moisture transport in atmospheric rivers*

Here, we introduce a new visualization of the coherence and overlap of the WV from the various source areas in a compact fashion. To display the dominant evaporation sources in a two-dimensional plot, the vertically integrated water vapor was calculated separately for each tracer and, then, expressed in percent relative to the total IWV. To show the coherence and overlap of the tracers in different regions of the model domain, the IWV contributions for each tracer were composited with transparent shading. Figure 6 shows the percent contribution of the various tracers to IWV below 500 hPa with transparent color shading. Each panel thereby presents an instantaneous snapshot of the water vapor tracer composition of the atmosphere. More intense shading of the same color denotes that a higher fraction of the same tracer contributes to the total IWV. When viewed jointly with plots of IWV (Fig. 3, right column), it can be identified what share the tracers contribute to the total IWV at each location. For reference to the IWV maps, the 14-mm IWV contour is shown as a thick black line on the composite maps. When viewed as a time lapse sequence, the various transparent shadings allow us to follow the evolution of the tracers. These maps are available for the entire simulation period and in different subsets of tracers in the online supplemental material.

TABLE 3. Mean 2-m temperature T_{2m} and precipitation P during atmospheric river (AR) and non-AR conditions (nAR) in the NN and SN domains calculated from 6-h model simulation data.

	T_{2m} AR (°C)	T_{2m} nAR (°C)	P AR (mm day^{-1})	P nAR (mm day^{-1})
NN	−0.85 ± 1.66	−2.22 ± 2.96	3.73 ± 3.24	3.44 ± 2.71
SN	2.37 ± 1.51	0.53 ± 1.42	5.55 ± 4.89	2.67 ± 2.01

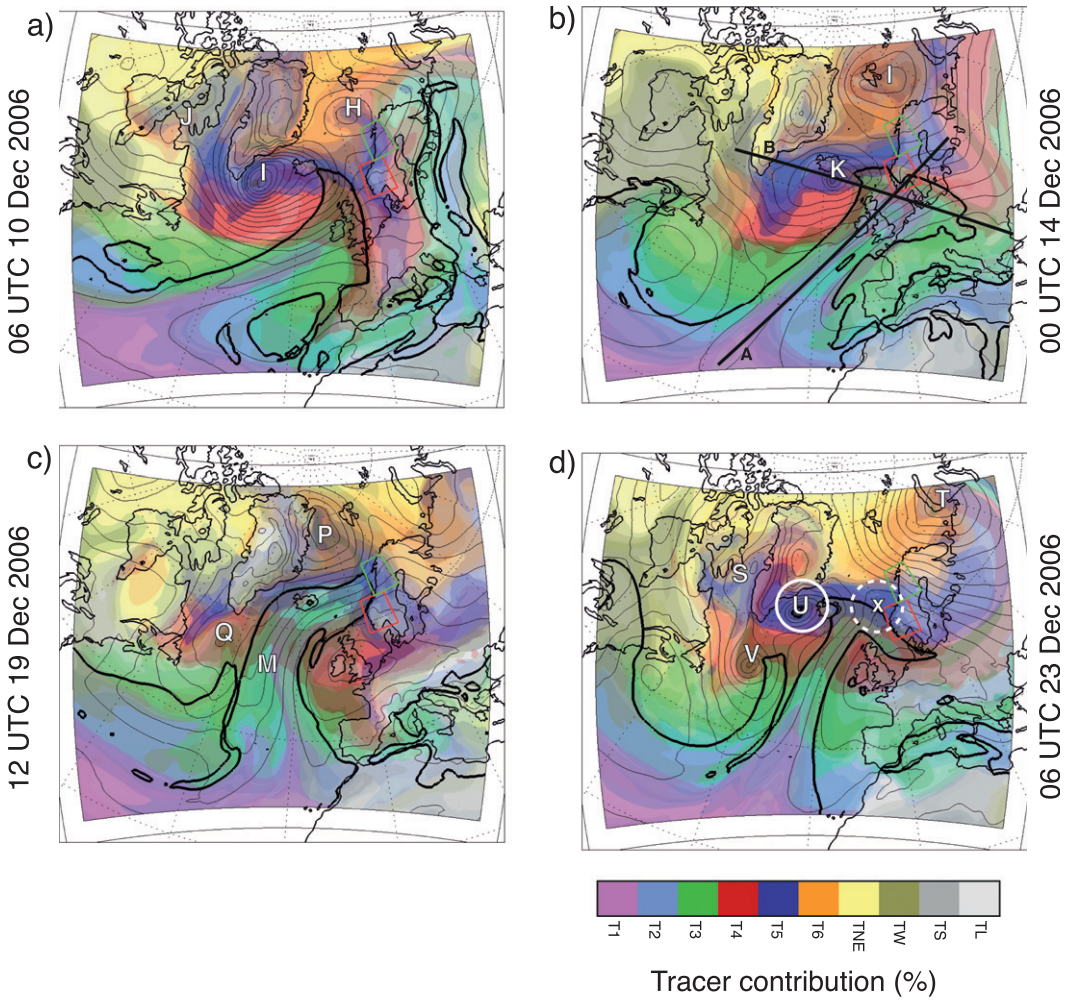

FIG. 6. Tracer composition of total IWV below 500 hPa (shaded) for the same times as in Fig. 3. More opaque shading indicates more than 10%, 30%, and 50% IWV contributions. SLP (gray contours, contour interval of 5 hPa) and cyclone symbols as in Fig. 3. Thick black contour denotes IWV of 14 mm. White solid and dashed circles around cyclone U and the X indicate a 500-km analysis radius (see text for details).

At 0600 UTC 10 December, the single large cyclone I dominated the SLP pattern in the domain. A broad AR was located southeast, with a strong northeasterly flow behind the cold front, as well as a zonally oriented upper-level jet axis (Figs. 3a,b). The tracer composition for this instance in time shows a mostly zonal distribution of moisture sources near the center of cyclone I, coincident with the respective tracer sources in the North Atlantic (Fig. 6a, cf. also Fig. 1). Substantial amounts of lower-latitude moisture advection interrupt the zonal moisture distribution in the AR area, over the British Isles from tracer T3, and near the Azores from tracers T1 and T2.

At 0000 UTC 14 December, a long, narrow AR was present in the eastern North Atlantic, oriented in the southwest–northeast direction, and underneath a strong upper-level jet (Figs. 3a,b). The tracer composition shows a prominent excursion of southerly tracers in the AR area, with blue shades from tracer T2 reaching all the way to southern Norway (Fig. 6b). In south-to-north progression, contributions from tracers TS (gray), T1 (pink), T2 (light blue), and T3 (light green) dominate the composition of the AR. The excursion covers about 10°–20° latitude for the successive tracers, pointing toward the loss of the WV due to precipitation, as the moist air is lifted during northward advection. In the areas west of the AR (the cold sector of the cyclone) where the low-level flow is weaker and has a northwesterly orientation, the moisture source composition is dominated by the respective local tracers.

A vertical cross section of specific humidity along the AR's axis at 0000 UTC 14 December (coordinates 25°N, 39°W and 63°N, 30°E; line S1 in Fig. 3d) shows that most

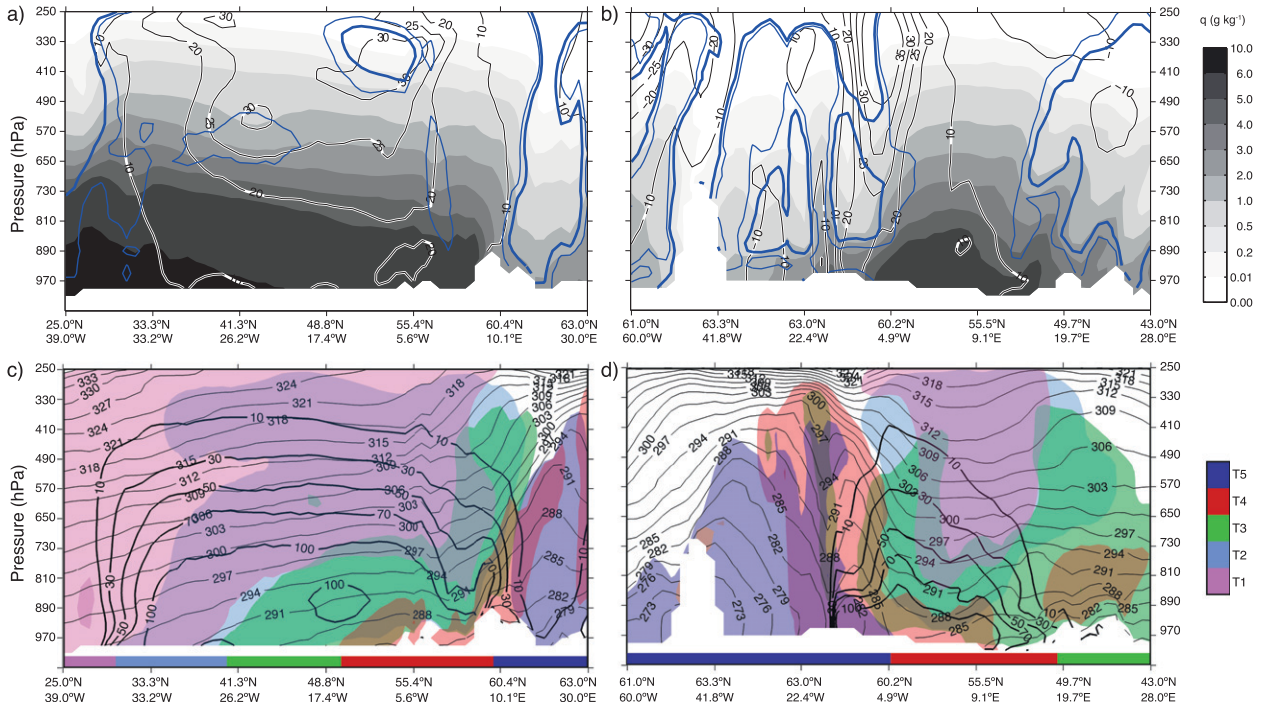

FIG. 7. Vertical cross sections of specific humidity (q, g kg^{-1}, shading), zonal–meridional wind speed (m s^{-1}, black contours), and relative humidity (80% and 90%, blue contours) at 0000 UTC 14 Dec 2006 along (a) 25°N, 39°W and 63°N, 30°E and (b) 61°N, 60°W and 43°N, 28°E, as indicated in Figs. 3d and 5b. (c),(d) Oceanic tracer fractions (shading, 10% contribution) and meridional moisture fluxes (g m^{-2} s^{-1}, boldface lines), and isentropes (K, thin lines) along the same transects as in (a),(b). For clarity only five oceanic tracers at one opacity level are shown in (c) and (d). Colored bars below the topography indicate the tracers evaporating at the surface.

of the WV resides at levels below 750 hPa with $q >$ ~5 g kg^{-1} (Fig. 7a, shading). This corresponds well with the finding by Ralph et al. (2005) based on 19 soundings of AR events that 75% of the water vapor transport in ARs takes place below ~800 hPa. North of 58°N the humidity values drop quickly, marking the northern edge of the occluded front. Substantial amounts of humidity persist throughout the troposphere, and with few exceptions the air mass is cloudy (RH > 80%, thick blue contour). High meridional wind velocities reach all the way from the upper troposphere to the surface, in particular toward the north end of the cross section with ~15–20 m s^{-1} between 45° and 57°N (Fig. 7a, solid black contours), leading to strong meridional moisture advection in the lower to middle troposphere (Fig. 7c). The corresponding tracer composition for the oceanic tracers (Fig. 7c, shading, cf. Fig. 6b) shows that at levels below ~850 hPa, the local tracers T1–T4 dominate in south-to-north sequence (colored boxes at the bottom indicate local source tracers), while the tracer contribution slopes northward vertically. This creates at most locations a vertical gradient of the tracer composition: toward higher levels progressively more remote tracers with southerly origin dominate (e.g., at 46°N, T3 up to 900 hPa, T2 up to 650 hPa, and T1 above 650 hPa). The tracer air masses thereby seem to follow or slightly exceed the sloping of the isentropes toward the north (e.g., T3 between 39° and 59°N). The initial rapid ascent of tracers (e.g., for tracer T2 in Fig. 7c) suggests that water vapor tracer is ventilated from the boundary layer into the WCB inflow and could be regarded as a WCB footprint region (Sinclair et al. 2008).

A second vertical cross section through the cyclone center and the head of the AR (coordinates 61°N, 60°W and 43°N, 28°E; line S2 in Fig. 3d) shows the difference between cold and warm sector air masses (Fig. 7b). The AR begins east of ~10°W, where a strong meridionally oriented jet at tropopause levels almost reaches to the surface, again with velocities of 10–20 m s^{-1} (black contours; cf. also Fig. 3c). The maximum poleward water vapor flux is located at the intersection between the moist air masses and high wind velocities (Fig. 7d, thick contours). To the west of this jet structure, specific humidities are lower at all levels, and the cloud cover becomes broken with RH < 80% (thick blue contour). The cyclone center is also located just west of the jet structure (62°N, 15°W; see Fig. 3d). The tracer composition for this cross section (Fig. 7d) shows that WV of local origin (T5) dominates west of the cyclone center, while the cyclone core itself contains a mixture of tracer T5

and T4 (Fig. 6b). Directly east of the upper-level jet, a very pronounced change in moisture tracer composition occurs, including substantial fractions of the southerly tracers T1–T3. The tracers form a vertical stack, starting with tracer T3 from 970 to 730 hPa, T2 from 950 to 260 hPa, and T1 from 820 to the top of the model atmosphere. The stack is more clearly visible if tracer contributions larger than 10% are inspected at the same cross section (not shown). Considering the high isentrope levels that these vapor contributions are found at compared to the potential temperatures near the surface for the evaporation region of the tracers, further processes must have lifted the WV to higher altitudes. While we expect that diabatic heating due to large-scale ascent is responsible for most of the vertical lifting at that time of the year, it is possible that at southerly latitudes convective mixing contributed to the spread of the tracer across a wider range of potential temperatures, as has been observed by Purvis et al. (2003). Note also that the tropopause has been lifted clearly in the region above the moisture flux maximum at 300 hPa in a wide area. In combination with the proximity to the jet structure, this suggests that the cyclone's WCB has been intersected at this location (Eckhardt et al. 2004; Roiger et al. 2011). At this instance in time, tracers T1 and T2 contribute to the WCB outflow near the tropopause, while tracer T3 mostly contributes to the meridional transport at midlevels. It is interesting to note the fairly clear vertical separation between the air masses, which may have been enhanced during northward advection by the more intense diabatic heating in the more warm and moist southerly air masses.

At 0600 UTC 19 December, a major, meridionally oriented AR extended far into the northern latitudes (Fig. 3f). The tracer composition for this situation shows a substantial disruption of the zonal tracer distribution by the AR (Fig. 6c), with a meridional progression of tracer distributions similar to what has been identified in Fig. 7. However, T2 is dominant even up to Iceland. Tropical cyclone M, which had been incorporated into this AR near 50°N, 35°W, at 1200 UTC 19 December, further enhanced the fraction of southerly tracers (Fig. 3f). Cyclone P, which was located southwest of Svalbard near 77°N at that time, had incorporated substantial amounts of moisture from 60° to 70°N (dark blue shading extending toward NE Greenland), yet tracer T2 also contributed more than 10% to the moisture in the occlusion.

At 1800 UTC 23 December, cyclones U and V were located south of Greenland, with their frontal bands joining to form one large AR (Fig. 3h). The eastern AR, mostly associated with cyclone U, shows again a meridional sequence of the different tracer contributions from south to north (Fig. 6d). The western AR associated with cyclone V is in its initial formation phase. As the joint analysis of the IWV map and the tracer composition reveals, in some regions substantial amounts of moisture added by this frontal band originate from local evaporation due to airmass transformation in the cold sector. It is important to note here that the ARs are not exclusively formed by meridional advection, but also by zonal advection and evaporation occurring en route. Near the centers of cyclones U and V, the local tracer corresponding to the current latitude of the cyclone dominates the moisture composition.

As indicated by the 14-mm IWV contours in Fig. 6, there is typically a substantial separation, on the order of 1000 km or more, between the cyclone center and the location where the poleward moisture transport is strongest (see also Fig. 7b). This finding is also consistent with results from an AR climatology (Neiman et al. 2008) and cyclone-centered composites of IWV in the North Atlantic (Rudeva and Gulev 2011). In the following section, it is examined how airmass properties in the cyclone center and at a location within the AR region east of the center change during a cyclone's life cycle.

f. Moisture composition changes in the vicinity of a cyclone

Based on SLP and absolute vorticity at 850 hPa, cyclone centers were manually tracked at 6-h intervals for the simulation period. In total, 29 individual cyclones were present and tracked in the model domain during December 2006. We focus our analysis here on cyclone U, which was associated with a well-defined frontal system and AR (Figs. 3f, 6d). The track of cyclone U starts farther south than for most other cyclones during this month (not shown). The minimum sea level pressure, vertically integrated latent and sensible heat energy, and moisture tracer composition were extracted in a 500-km radius around the cyclone center along the track at each 6-h time interval (solid white circle in Fig. 6d). Latent heat (LH) and sensible heat (SH) energy content were calculated following Oort (1971) by vertically and horizontally integrating $\mathrm{LH} = c_p \times T$ and $\mathrm{SH} = L \times q$ within the given radius, where c_p is the specific heat at constant pressure, L is the heat of condensation, and q is specific humidity.

Cyclone U was initially tracked at 1200 UTC 20 December at 37°N (Fig. 8a). During the following 4 days, it fairly continually progressed up to 70°N, reaching a core pressure minimum of 977 hPa at 0600 UTC 23 December at ~64°N (Fig. 6d, solid white circle; see also Fig. 3f). The vertically integrated sensible and latent heat energy content in the core of the cyclone continuously decreased as the cyclone was intensifying and

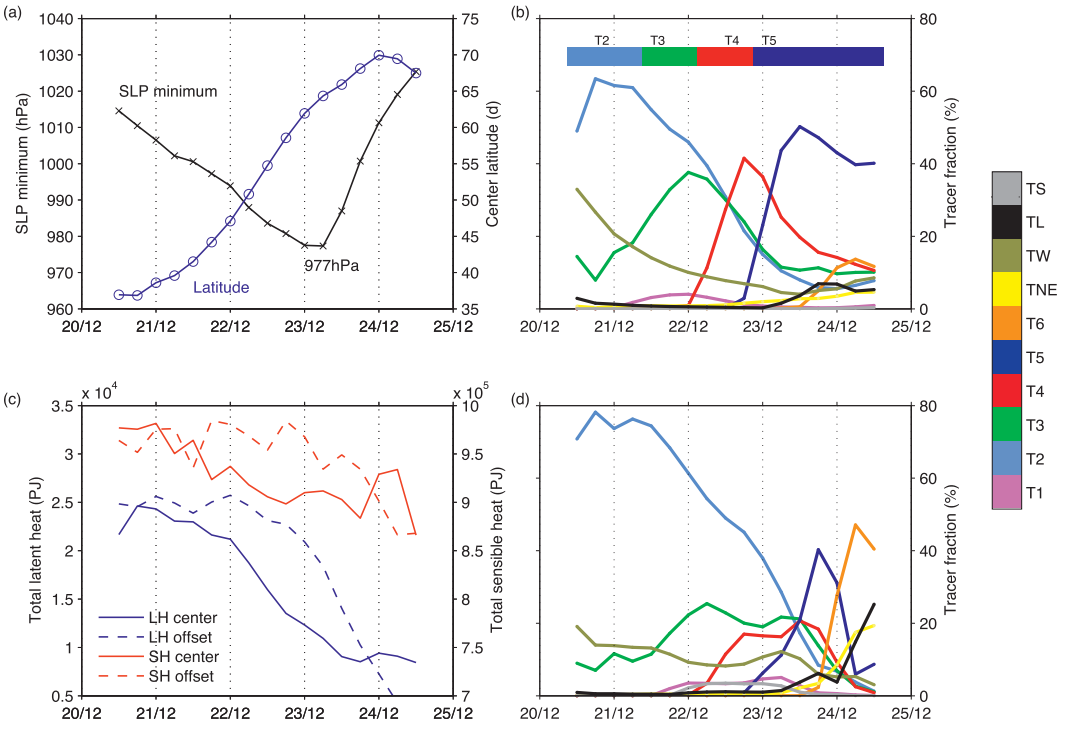

FIG. 8. Time series of quantities analyzed within a 500-km radius about the cyclone center defined as the minimum SLP for cyclone U. (a) SLP minimum (hPa, black line) and center latitude (in ° latitude, blue line). (b) Fractional tracer contribution to total IWV in the analysis area (%, solid lines). Colored bar indicates the tracer evaporating from the ocean underneath the cyclone center at a given time. (c) Area-integrated latent heat [petajoules (PJ), blue lines] and sensible heat (PJ, red lines) for the cyclone center region (solid lines) and with a 1000-km offset toward the east (dashed lines). (d) As in (b), but for the analysis region with a 1000-km offset toward the east.

moving poleward (Fig. 8c, solid lines). During the strongest intensification phase on 22 December, the latent heat content decreased more rapidly than the sensible heat content, indicating heat supply by condensation processes. The minimum energy content was reached 12 h after the minimal core pressure at 1200 UTC 23 December, before the cyclone started to decay and disappeared from the SLP chart at 0600 UTC 24 December. Note that due to the fixed 500-km radius, Fig. 8c does not depict the energy content of the complete cyclone.

The contributions by the WV tracers during the life cycle of cyclone U show a rapid transformation over time (Fig. 8b). During the first 24 h, most of the moisture (up to 62%) in the cyclone core originated from 30° to 40°N (T2), while contributions from the southern boundary tracer TS decreased rapidly (from ~38% to 10%) and those from T3 started to increase (from ~10% to 20%). As the cyclone continued moving north, incorporation of moisture from tracers T3, T4, and T5 in sequence replaced the more southerly tracers and dominated the moisture composition in the cyclone. As indicated by the colored bars at the top of Fig. 8b, the contribution of each of the more northerly tracers reached a maximum within 24 h of moving over the respective evaporation source. This highlights the rapid turnover of latent heat energy in the cyclone center, in particular during the strongest intensification phase on 22 December (Fig. 8c).

To investigate how the tracers progressed in the AR associated with the cyclone, the analysis was repeated for a location offset 1000 km to the east of the cyclone center, near the maximum of the meridional transport (Fig. 6d, dashed circle; cf. also Fig. 3h). The tracer composition is markedly different compared to the cyclone center. Tracer T2 dominates the AR until the end of the intensification phase, together with smaller contributions from TS and T3 (Fig. 8d). At this point (0000 UTC 24 December), the air mass contains equal contributions from tracers T2 to T5, and thereafter is dominated by T5 and T6 in sequence. Thus, the tracer composition in the AR area is clearly dominated by the continuous long-range advection of tracers T2 and TS. Rather than becoming dominant, local tracers contribute at most 20% to the WV in the air mass, which may be partly from evaporation and partly from zonal advection (see section 3e).

The total latent heat content above the offset area correspondingly decreases slower than in the cyclone center and, in fact, remains nearly constant until the phase of strongest cyclone intensification (Fig. 8c, dashed blue line). The sensible heat content remains higher than in the cyclone center, reflecting the warmer temperatures in the AR region (Fig. 8c, dashed red line). Similar transformations of the air mass in the cyclone core and the associated AR region can be identified for many of the poleward-progressing cyclones tracked during December 2006 (not shown).

The mean meridional moisture transport from the oceanic source areas throughout the analysis period of December 2006 is investigated by the zonal mean fractional contribution of each tracer to total precipitation (Fig. 9). Each oceanic tracer (T1–T6) dominates locally with 60%–35%. It is interesting to note the skewed shape of the contributions, which are similar for each tracer, marked by a steep decline toward more southerly latitudes, barely extending farther than 10° latitude, and having a long tail toward the north. For tracers T2 and T3, the tail extends more than 30° latitude poleward at a contribution of ~10%. This shape is most likely a result of moisture being preferentially transported northward from the southern midlatitudes and subtropics where evaporation is strongest (Trenberth and Guillemot 1998). Together with the reduced size of the tracer area toward the north (Fig. 1), the long tails contribute to the decreased tracer concentration maxima with increasing latitude. During December 2006, much of this mean northward moisture transport occurred in the form of distinct and pronounced ARs.

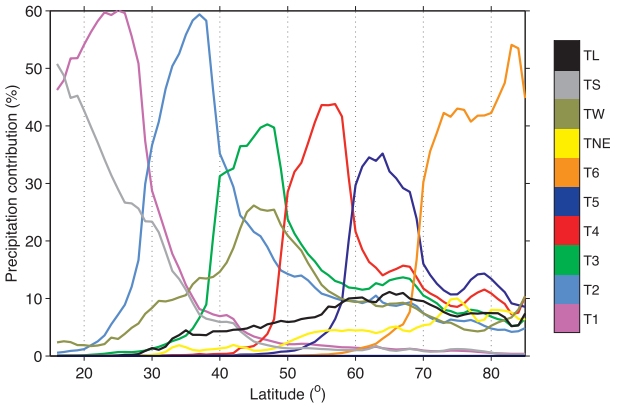

FIG. 9. Zonal mean of the precipitation fraction contributed by each water tracer during December 2006 (%, solid lines) as a function of latitude.

4. Discussion

Four interesting observations with regard to the formation of ARs have been made in this study. First, the formation of ARs was tightly coupled to the predominant circulation at tropopause levels. Second, individual cyclones seemed to contribute to the formation and maintenance of ARs at the trailing end by adding moisture accumulated at their cold fronts. Third, cyclones use a part of ARs as a reservoir to feed their WCB airstream. Fourth, individual ARs could be maintained or depleted by several cyclones in temporal sequence.

Several of these observations are at odds with the traditional view that WCBs and ARs are two terms for the same feature in different frameworks. WCBs are connected to the intensification of a single cyclone, leading to the loss of moisture from the atmosphere by rapid ascent within a few days. They are thus spatially and temporally constrained, coherent airstreams. ARs in contrast can cover fairly large, sometimes irregular, areas that will not all ascend in a WCB-like fashion; their lifetimes can exceed that of a cyclone; and they can be maintained or depleted by more than one cyclone sequentially. This underlines that an AR needs to be distinguished from a WCB. Eckhardt et al. (2004) pointed out that the WCB is the main sink process of precipitable water in the midlatitudes. Given the interrelation between WCBs and ARs found in this study, the joint analysis of both features appears as a promising direction for future research.

Figure 10 schematically summarizes these findings. When a pronounced wave pattern is present at upper levels, resembling the anticyclonic (LC1) life cycle (Fig. 10a, white dashed line), the meridional jet orientation enhances the poleward advection throughout the troposphere, leading to the formation of sometimes irregular-shaped ARs (Fig. 10a, colored areas). Due to advection of the air masses along moist adiabats, a vertical stack of WV is thereby formed with WV originating from lower latitudes residing at higher altitudes. At the western edge of the AR, small cyclones develop from frontal waves. Their cold fronts add moisture to the AR by zonal advection. At the same time, the cyclones tap the moisture available from the AR region for their WCB airstream, thus contributing to the AR at one end and feeding of it for their spinup and development at the other. Subsequent cyclones thus profit from the moisture transported poleward by previous cyclones, leading to a ''handover'' of moisture between subsequent short-lived cyclones. This implies that an AR is distinct from a cyclone's WCB when it persists sufficiently long for several small cyclones to develop in sequence.

Similar joint action between sequential cyclones for advecting large amounts of moisture poleward has already been seen in an earlier study (Stohl et al. 2008). In

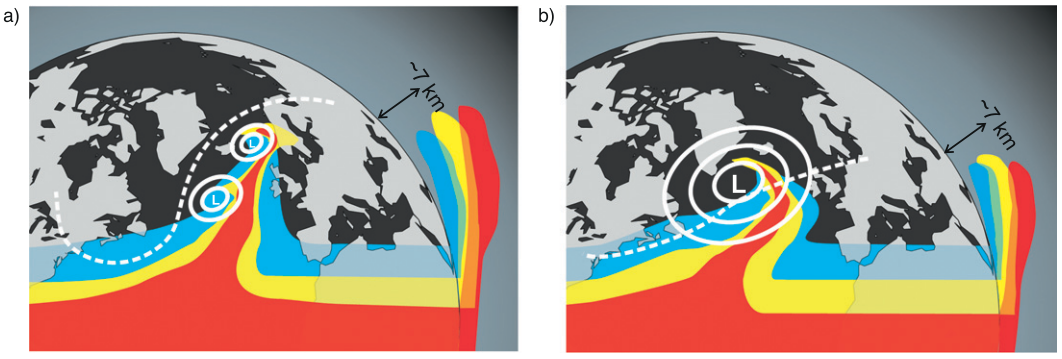

FIG. 10. Schematic view of the two moisture transport configurations. (a) Anticyclonic (LC1 like) wave breaking with a meridional upper-level jet and (b) cyclonic (LC2 like) wave breaking with a zonal upper-level jet. Dashed white line shows the orientation of the upper-level jet, solid white lines show SLP, and shaded colors indicate oceanic moisture of different latitudes. On the right-hand sides, quasi-vertical projections of the moisture tracers are shown. See text for details.

that study, a first cyclone brought along the moisture and the second one fed on it, thereby causing extreme precipitation in southern Norway. It thus seems that major ARs, especially those extending to very high latitudes, may need more than one cyclone to first be transported far north and then to be precipitated out.

A weak wave pattern at the tropopause, resembling the LC2 life cycle, leads to predominantly zonal flow throughout the troposphere (Fig. 10b, white dashed line). In this case a single, slow-moving, large cyclone develops, with more limited poleward advection of moisture to lower altitudes, as the AR is slowly advected eastward. During this type of development, the distinction between an AR and the cyclone's WCB airstream may be difficult to determine near the cyclone, and may be more in line with the dominating view until now, in which the WCB is identical to or the end point of an AR (Eckhardt et al. 2004).

5. Conclusions

In this study, we applied a WV tagging approach to gain new insight into the processes leading to heavy precipitation in western Scandinavia and, more generally, of WV transport due to extratropical cyclones during winter. This study covers one single month (December 2006), and our results can to some extent only be indicative of midlatitude moisture transport processes in general. Nevertheless, new process understanding has been obtained from this study, which warrants corroboration on longer time scales and by a larger number of cases to attain a more general validity.

During periods of high IWV over Norway, precipitation had more southerly moisture sources and was associated with larger daily precipitation totals. These periods were coincident with impinging atmospheric rivers, excursions of warm and moist air from subtropical and southern midlatitudes. High wind velocities along the ARs, aligned with the upper-level jet, translated water vapor from a wide range of southerly latitudes poleward. Vertical cross sections through an AR revealed a vertical stack of the tracer composition, with more southerly moisture residing at higher altitudes. The cyclone cores instead quickly adjusted to the local tracer composition by rapid moisture turnover.

The ARs studied here could persist for an extended period of time, partly without being related to one particular cyclone. ARs could be maintained by advection of bands of high IWV and depleted by WCBs or interception with the steep orography along the Norwegian west coast. The ARs mostly coincided with a southwest–northeast-oriented tropopause jet, pointing toward a leading role of the upper-level circulation for setting poleward moisture transport. A more meridionally oriented jet favored both stronger moisture advection from southern latitudes and the occurrence of smaller, short-lived cyclones as compared to a more zonally oriented jet and larger cyclones. Poleward moisture (and energy) transport was thus directly related to the leading wave breaking pattern.

To this point, it had been assumed that WCBs are mostly coincident with ARs or at least that a WCB would constitute an AR's end point where most of the moisture is precipitated during ascent. Given that ARs can be associated with several cyclones, as well as their persistence, the coupling to the upper-level jet, and their role as a reservoir depleted by sometimes more than one single cyclone's WCB airstream, ARs and WCBs should be considered as distinct but related entities.

The sequential interaction between cyclones along an AR could have important implications for numerical

weather prediction, since the precipitation amount may be determined by the joint transport of several (rather than a single) cyclones. Data assimilation for instance may be very sensitive to even small errors in the analyzed position of cyclones, potentially leading to excessive or too little loss of WV from the atmosphere if the position of the cyclone center relative to the AR is not captured accurately enough.

Further analysis is under way to expand the study to a longer time frame and to quantify the contribution of individual and interacting cyclones to the high-latitude energy budget.

Acknowledgments. We thank the three reviewers for their detailed and constructive comments. Heini Wernli is acknowledged for helpful comments on the manuscript. The Norwegian Meteorological Service met.no is thanked for access to the eKlima station database and access to the ECMWF analysis data. This study was supported by the Norwegian Research Council as part of the projects Where Norway Receives Its Water From (Project 172707/S30) and POCAHONTAS (Project 178345/S30).

REFERENCES

Bao, J.-W., S. A. Michelson, P. J. Neiman, F. M. Ralph, and J. M. Wilczak, 2006: Interpretation of enhanced integrated water vapor bands associated with extratropical cyclones: Their formation and connection to tropical moisture. *Mon. Wea. Rev.,* **134,** 1063–1080.

Benestad, R. E., and A. Melsom, 2002: Is there a link between the unusually wet autumns in southeastern Norway and sea-surface temperature anomalies? *Climate Res.,* **23,** 67–79.

Bjerknes, J., 1919: On the structure of moving cyclones. *Mon. Wea. Rev.,* **47,** 95–99.

Bosilovich, M. G., and S. D. Schubert, 2002: Water vapor tracers as diagnostics of the regional hydrologic cycle. *J. Hydrometeor.,* **3,** 149–165.

Boutle, I. A., S. E. Belcher, and R. S. Plant, 2011: Moisture transport in midlatitude cyclones. *Quart. J. Roy. Meteor. Soc.,* **137,** 360–373.

Browning, K. A., 1990: Organization of clouds and precipitation in extratropical cyclones. *Extratropical Cyclones: The Erik H. Palmén Memorial Volume,* C. Newton and E. Holopainen, Eds., Amer. Meteor. Soc., 129–153.

Carlson, T. N., 1980: Airflow through midlatitude cyclones and the comma cloud pattern. *Mon. Wea. Rev.,* **108,** 1498–1509.

Cattiaux, J., R. Vautard, and P. Yiou, 2009: Origins of the extremely warm European fall of 2006. *Geophys. Res. Lett.,* **36,** L06713, doi:10.1029/2009GL037339.

Dickinson, R. E., 1984: Modeling evapotranspiration for 3-dimensional global climate models. *Climate Processes and Climate Sensitivity, Geophys. Monogr.,* Vol. 29, Amer. Geophys. Union, 58–72.

Eckhardt, S., A. Stohl, H. Wernli, P. James, C. Forster, and N. Spichtinger, 2004: A 15-year climatology of warm conveyor belts. *J. Climate,* **17,** 218–237.

Harrold, T. W., 1973: Mechanisms influencing the distribution of precipitation within baroclinic disturbances. *Quart. J. Roy. Meteor. Soc.,* **99,** 232–251.

Joussaume, J., R. Sadourny, and J. Jouzel, 1984: A general circulation model of water isotope cycles in the atmosphere. *Nature,* **311,** 24–29.

Kessler, E., 1969: *On the Distribution and Continuity of Water Substance in Atmospheric Circulations. Meteor. Monogr.,* No. 32, Amer. Meteor. Soc., 84 pp.

Knippertz, P., and J. E. Martin, 2007: A Pacific moisture conveyor belt and its relationship to a significant precipitation event in the semiarid southwestern United States. *Wea. Forecasting,* **22,** 125–144.

——, and H. Wernli, 2010: A Lagrangian climatology of tropical moisture exports to the Northern Hemispheric extratropics. *J. Climate,* **23,** 987–1003.

Koster, R., J. Jouzel, R. Souzzo, G. Russell, W. Broecker, D. Rind, and P. Eagleson, 1986: Global sources of local precipitation as determined by the NASA/GISS GCM. *Geophys. Res. Lett.,* **13,** 121–124.

Lavers, D. A., R. P. Allan, E. F. Wood, G. Villarini, D. J. Brayshaw, and A. J. Wade, 2011: Winter floods in Britain are connected to atmospheric rivers. *Geophys. Res. Lett.,* **38,** L23803, doi:10.1029/2011GL049783.

Lin, Y.-L., R. D. Farley, and H. D. Orville, 1983: Bulk parameterization of the snow field in a cloud model. *J. Climate Appl. Meteor.,* **22,** 1065–1092.

Luterbacher, J., M. A. Liniger, A. Menzel, N. Estrella, P. M. Della-Marta, C. Pfister, T. Rutishauser, and E. Xoplaki, 2007: Exceptional European warmth of autumn 2006 and winter 2007: Historical context, the underlying dynamics, and its phenological impacts. *Geophys. Res. Lett.,* **34,** L12704, doi:10.1029/2007GL029951.

Majewski, D., 1991: The Europa-Modell (EM) of the Deutscher Wetterdienst. *Proc. Seminar on Numerical Methods in Atmospheric Models,* Vol. 2, Reading, United Kingdom, ECMWF, 147–191.

Meteorologisk Institutt, 2007: Vaeret i norge, klimatologisk maanedsoversikt desember 2006. Norwegian Meteorological Institute Public Records 12/2006, 18 pp.

Neiman, P. J., F. M. Ralph, G. A. Wick, Y.-H. Kuo, T.-K. Wee, Z. Ma, G. H. Taylor, and M. D. Dettinger, 2008: Diagnosis of an intense atmospheric river impacting the Pacific Northwest: Storm summary and offshore vertical structure observed with COSMIC satellite retrievals. *Mon. Wea. Rev.,* **136,** 4398–4420.

——, L. J. Schick, F. M. Ralph, M. Hughes, and G. A. Wick, 2010: Flooding in western Washington: The connection to atmospheric rivers. *J. Hydrometeor.,* **12,** 1337–1358.

Newell, R. E., N. E. Newell, Y. Zhu, and C. Scott, 1992: Tropospheric rivers?—A pilot study. *Geophys. Res. Lett.,* **19,** 2401–2404.

Numaguti, A., 1999: Origin and recycling processes of precipitating water over the Eurasian continent: Experiments using an atmospheric general circulation model. *J. Geophys. Res.,* **104,** 1957–1972.

Oort, A. H., 1971: The observed annual cycle in the meridional transport of atmospheric energy. *J. Atmos. Sci.,* **28,** 325–339.

Osborn, T. J., K. R. Briffa, S. F. B. Tett, P. D. Jones, and R. M. Trigo, 1999: Evaluation of the North Atlantic Oscillation as simulated by a coupled climate model. *Climate Dyn.,* **15,** 685–702.

Purvis, R., and Coauthors, 2003: Rapid uplift of nonmethane hydrocarbons in a cold front over central Europe. *J. Geophys. Res.,* **108,** 4224, doi:10.1029/2002JD002521.

Ralph, F. M., P. J. Neiman, and G. A. Wick, 2004: Satellite and CALJET aircraft observations of atmospheric rivers over the eastern North Pacific Ocean during the winter of 1997/98. *Mon. Wea. Rev.,* **132,** 1721–1745.

——, ——, and R. Rotunno, 2005: Dropsonde observations in low-level jets over the northeastern Pacific Ocean from CALJET-1998 and PACJET-2001: Mean vertical-profile and atmospheric-river characteristics. *Mon. Wea. Rev.,* **133,** 889–910.

——, ——, G. A. Wick, S. I. Gutman, M. D. Dettinger, D. R. Cayan, and A. B. White, 2006: Flooding on California's Russian River: Role of atmospheric rivers. *Geophys. Res. Lett.,* **33,** L13801, doi:10.1029/2006GL026689.

——, ——, G. N. Kiladis, and K. Weickmann, 2011: A multiscale observational case study of a Pacific atmospheric river exhibiting tropical–extratropical connections and a mesoscale frontal wave. *Mon. Wea. Rev.,* **139,** 1169–1189.

Roiger, A., and Coauthors, 2011: In situ observation of Asian pollution transported into the Arctic lowermost stratosphere. *Atmos. Chem. Phys.,* **11,** 10 975–10 994, doi:10.5194/acp-11-10975-2011.

Rudeva, I., and S. K. Gulev, 2011: Composite analysis of North Atlantic extratropical cyclones in NCEP–NCAR reanalysis data. *Mon. Wea. Rev.,* **139,** 1419–1446.

Schär, C., D. Lüthi, U. Beyerle, and E. Heise, 1999: The soil precipitation feedback: A process study with a regional climate model. *J. Climate,* **12,** 722–741.

Sinclair, V. A., S. L. Gray, and S. E. Belcher, 2008: Boundary-layer ventilation by baroclinic life cycles. *Quart. J. Roy. Meteor. Soc.,* **134,** 1409–1424, doi:10.1002/qj.293.

Smolarkiewicz, P. K., 2006: Multidimensional positive definite advection transport algorithm: An overview. *Int. J. Numer. Methods Fluids,* **50,** 1123–1144.

Sodemann, H., 2006: Tropospheric transport of water vapor: Lagrangian and Eulerian perspectives. Ph.D. dissertation, Swiss Federal Institute of Technology, 230 pp.

——, H. Wernli, and C. Schwierz, 2009: Sources of water vapor contributing to the Elbe flood in August 2002—A tagging study in a mesoscale model. *Quart. J. Roy. Meteor. Soc.,* **135,** 205–223.

Steensen, B. M., H. Ólafsson, and M. O. Jonassen, 2011: An extreme precipitation event in central Norway. *Tellus,* **63,** 675–686.

Stohl, A., C. Forster, and H. Sodemann, 2008: Remote sources of water vapor forming precipitation on the Norwegian west coast at 60°N—A tale of hurricanes and an atmospheric river. *J. Geophys. Res.,* **113,** D05102, doi:10.1029/2007JD009006.

Thorncroft, C., B. Hoskins, and M. McIntyre, 1993: Two paradigms of baroclinic-wave life-cycle behavior. *Quart. J. Roy. Meteor. Soc.,* **119,** 17–55.

Tiedtke, M., 1989: A comprehensive mass flux scheme for cumulus parameterization in large-scale models. *Mon. Wea. Rev.,* **117,** 1779–1800.

Trenberth, K. E., 1999: Atmospheric moisture recycling: Role of advection and local evaporation. *J. Climate,* **12,** 2366–2387.

——, and C. J. Guillemot, 1998: Evaluation of the atmospheric moisture and hydrological cycle in the NCEP/NCAR reanalyses. *Climate Dyn.,* **14,** 213–231.

Wernli, H., 1997: A Lagrangian-based analysis of extratropical cyclones. II: A detailed case-study. *Quart. J. Roy. Meteor. Soc.,* **123,** 1677–1706.

Winschall, A., 2012: Evaporative moisture sources for heavy precipitation events. Ph.D. dissertation, Swiss Federal Institute of Technology, 152 pp.

——, S. Pfahl, H. Sodemann, and H. Wernli, 2012: Impact of North Atlantic evaporation hot spots on southern Alpine heavy precipitation events. *Quart. J. Roy. Meteor. Soc.,* **138,** 1245–1258, doi:10.1002/qj.987.

Zhu, Y., and R. E. Newell, 1998: A proposed algorithm for moisture fluxes from atmospheric rivers. *Mon. Wea. Rev.,* **126,** 725–735.